

Heavy-light mesons from a flavour-dependent interaction

Fei Gao^a, Angel S. Miramontes^b, Joannis Papavassiliou^{b,d}, Jan M. Pawłowski^{c,d}

^a*School of Physics, Beijing Institute of Technology, Beijing, 100081, China*

^b*Department of Theoretical Physics and IFIC, University of Valencia and CSIC, Valencia, E-46100, Spain*

^c*Institut für Theoretische Physik, Universität Heidelberg, Philosophenweg 16, Heidelberg, 69120, Germany*

^d*ExtreMe Matter Institute EMMI, GSI, Planckstrasse 1, Darmstadt, 64291, Germany*

Abstract

We introduce a new symmetry-preserving framework for the physics of heavy-light mesons, whose key element is the effective incorporation of flavour-dependent contributions into the corresponding bound-state and quark gap equations. These terms originate from the fully-dressed quark-gluon vertices appearing in the kernels of these equations, and provide a natural distinction between “light” and “heavy” quarks. In this approach, only the classical form factor of the quark-gluon vertex is retained, and is evaluated in the so-called “symmetric” configuration. The standard Slavnov-Taylor identity links this form factor to the quark wave-function, allowing for the continuous transition from light to heavy quarks through the mere variation of the current quark mass in the gap equation. The method is used to compute the masses and decay constants of specific pseudoscalars and vector heavy-light systems, showing good overall agreement with both experimental data and lattice simulations.

1. Introduction

The systematic description of heavy-light mesons within the framework of Quantum Chromodynamics (QCD) poses a significant challenge [1–15], mainly due to the substantial mass difference between their constituent quarks. Indeed, composed from one heavy (charm or bottom) and one light (up, down, or strange) valence quark, these mesons are less tractable by standard methods, such as the classic rainbow-ladder approximation and related approaches. The experimental determination of the heavy-light meson spectrum, and specifically the discovery of the narrow states $D_s(2317)$ [16–18] and $D_s(2460)$ [17–19], have attracted significant interest from both the theoretical and experimental communities. These states challenge traditional quark model predictions for heavy-light systems [20], in contrast to the better understood D meson states. Importantly, the heavy-light spectrum will be accessible in the later stages of PANDA [21], while other experiments, including LHCb [22, 23], BES III [24] and CMS [25], are conducting precise measurements of cross sections and decay processes involving heavy-light and heavy-heavy mesons.

The contemporary symmetry-preserving treatment of mesonic systems is based on the combined analysis of Schwinger-Dyson equations (SDEs), and in particular the quark gap equation, and Bethe-Salpeter equations (BSEs) [26–58]. This set of equations is supplied with a propagator-like interaction, typically in the form of effective charges or kindred quantities. It is clear, however, that, in order for flavour-effects to be properly taken into account, crucial contributions stemming from the fully-dressed quark-gluon vertices must be supplemented to the total interaction.

In the present work we incorporate such terms at the level of the “one-gluon exchange” interaction kernel. After the crucial skeleton expansion has been duly implemented, this particular

kernel contains two fully-dressed quark-gluon vertices, whose structure is simplified by retaining only their classical form factor, evaluated in the *symmetric configuration*. The Slavnov-Taylor identity (STI) [59, 60] allows us to express this form factor as the product of a universal component and the flavour-specific quark wave-function, whose form is determined from the corresponding gap equation. The combination of this universal component with the gluon propagator gives rise to a variant of the standard Taylor effective charge [61–65], which is enhanced by a factor of about 1.35 around the 1 GeV momentum region.

The subsequent convolution of this effective charge with the quark wave functions originating from each vertex leads to the final flavour-dependent interaction strength. Thus, the relevant flavour content is entirely determined from the gap equation, by adjusting appropriately the values of the current quark masses, with no need to resort to additional dynamical equations. Note also that, quite importantly, the propagator-like nature of this interaction preserves the crucial axial Ward-Takahashi identity (WTI) [30, 66], thus enforcing a massless pion in the chiral limit. We emphasize that the building blocks of our analysis, such as gluon and ghost propagators and the Taylor effective charge, are obtained from lattice QCD [65, 67], and are in excellent agreement with a multitude of functional studies, see, e.g., [44, 68–73]. In fact, no phenomenological parameter, such as the constituent quark mass or the strength of the vertex dressing, had to be adjusted from experiment.

The resulting interaction strength is used to estimate the masses and decay constants of several heavy-light systems, such as D , B , and η . The calculations are carried out for Euclidean momenta, and the physical values are obtained through an extrapolation algorithm. The results obtained compare very well with experiment and lattice QCD.

2. Gluons, quarks, and mesons within Landau-gauge QCD

Our analysis and computations are performed in *Landau-gauge* QCD. The main components used in this study are introduced below, as items (i)-(v):

(i) The gluon propagator, $\Delta_{\mu\nu}^{ab}(q^2) = -i\delta^{ab}\Delta_{\mu\nu}(q^2)$, with

$$\Delta_{\mu\nu}(q) = \Delta(q^2)P_{\mu\nu}(q), \quad \Delta(q^2) = \mathcal{Z}(q^2)/q^2, \quad (1)$$

where $P_{\mu\nu}(q) = \delta_{\mu\nu} - q_\mu q_\nu/q^2$ is the transverse projection operator, $\Delta(q^2)$ denotes the scalar component of the gluon propagator, and $\mathcal{Z}(q^2)$ the corresponding dressing function. At tree-level, $\Delta_{\mu\nu}^{(0)}(q) = P_{\mu\nu}(q)/q^2$, and so $\Delta_{\mu\nu}(q) = \mathcal{Z}(q^2)\Delta_{\mu\nu}^{(0)}(q)$.

(ii) The ghost propagator, denoted by $D^{ab}(q^2) = i\delta^{ab}D(q^2)$, and the corresponding dressing function, $F(q^2)$, defined as $D(q^2) = F(q^2)/q^2$.

(iii) The quark propagator, denoted by $S_f^{ab}(p) = i\delta^{ab}S_f(p)$, where the index f stands for the quark flavour, taking values $f = u, d, s, c, b$. The standard decomposition of $S_f^{-1}(p)$ is

$$S_f^{-1}(p) = i\not{p}A_f(p^2) + B_f(p^2), \quad (2)$$

where $A_f(p^2)$ and $B_f(p^2)$ are the dressings of the Dirac vector and scalar tensor structure, respectively. The renormalization-group invariant (RGI) quark mass function, $\mathcal{M}_f(p^2)$, is given by $\mathcal{M}_f(p^2) = B_f(p^2)/A_f(p^2)$. At tree-level, $S_{0,f}^{-1}(p) = i\not{p} + m_f$, where m_f is the current quark mass for the flavour f . Finally, the *self-energy*, $\Sigma(p^2)$, is defined as $\Sigma_f(p^2) = S_f^{-1}(p) - S_{0,f}^{-1}(p)$.

(iv) The fully-dressed quark-gluon vertex is written in the form

$$\mathbb{\Gamma}_f^{a\mu}(q, p) = ig \frac{\lambda^a}{2} \Gamma_f^\mu(q, p), \quad (3)$$

where a and μ are the colour and Lorentz indices respectively, and f denotes flavour. In addition, λ^a , with $a = 1, 2, \dots, 8$, are the Gell-Mann matrices, and g is the gauge coupling. Furthermore, q and p denote the incoming gluon and quark momenta respectively; the outgoing anti-quark momentum r is fixed by momentum conservation, $r = q + p$. At tree-level, the quark-gluon vertex reduces to $\Gamma_\mu^{(0)} = \gamma_\mu$ for all flavours.

(v) The *Taylor effective charge*, $\alpha_\tau(q^2)$, defined as [61–65]

$$\alpha_\tau(q^2) = \alpha_s \mathcal{Z}(q^2) F^2(q^2), \quad (4)$$

where $\alpha_s = g^2/4\pi$ is the Taylor coupling at the renormalization point $p^2 = \mu^2$ with $\mathcal{Z}(\mu^2)F^2(\mu^2) = 1$. Its modified version Eq. (19) constructed in Sec. 4 is one of the main building blocks in the present approach.

There are two main dynamical equations that are of central importance for this study, namely the quark gap equation that controls the evolution of the quark propagator, and the BSE that governs the formation of mesonic bound states.

In its renormalized form, the gap equation is given by

$$S^{-1}(p) = Z_2(i\not{p} + m_r) + Z_1 C_f g^2 \int_k \Gamma_\mu^{(0)} S(k) \Gamma_\nu(q, k) \Delta^{\mu\nu}(q), \quad (5)$$

where $q := p - k$, and $C_f = 4/3$ is the Casimir eigenvalue of the fundamental representation, and m is the current quark mass; the flavour index f has been suppressed for simplicity. Furthermore, $\int_k := (2\pi)^{-4} \int_{-\infty}^{+\infty} d^4k$, where the use of a symmetry-preserving regularization scheme is implicitly assumed. Finally, Z_1 and Z_2 are the renormalization constants of the quark-gluon vertex and the quark propagator, respectively. Note that Eq. (5) is complete, in the sense that it contains all possible quantum corrections.

In the meson BSE we will approximate the renormalized four-quark kernel \mathcal{K} by its one-gluon exchange form, $\overline{\mathcal{K}}$,

$$\overline{\mathcal{K}} = g^2 \left(Z_1 \Gamma_\mu^{(0)} \right) \Delta^{\mu\nu}(q) \Gamma_\nu(q, k). \quad (6)$$

In Eq. (6) we have paired the classical vertex with the renormalization factor, $Z_1 \Gamma_\mu^{(0)}$. This building block occurs in all SDEs and BSEs and will be treated within the skeleton expansion, see Sec. 3. Eq. (6) is precisely the kernel appearing in Eq. (5). In particular, the BSE reads

$$\mathcal{A}(p, P) = -g^2 \int_k \left(Z_1 \Gamma_\mu^{(0)} \right) \tilde{\mathcal{A}}(k, P) \Gamma_\nu(q, k) \Delta^{\mu\nu}(q), \quad (7)$$

where $\tilde{\mathcal{A}}(k, P) = S(k_1) \mathcal{A}(k, P) S(k_2)$, P denotes the total momentum of the meson, p represents the relative momentum between the quark and the anti-quark, k is the loop momentum, with $k_1 = k + P/2$ and $k_2 = k - P/2$. As in Eq. (6) we have singled out the universal building block $Z_1 \Gamma_\mu^{(0)}$. In the case of vector mesons, the corresponding BSE is obtained from Eq. (7) through the substitution $\mathcal{A}(p, P) \rightarrow \mathcal{A}^\mu(p, P)$.

3. Skeleton expansion

It is well-known, that an effective charge, such as $\alpha_\tau(q^2)$, emerges naturally inside a one-gluon exchange amplitude if the gluon propagator can be combined with momentum-dependent contributions from *both* vertices it is attached to [42, 74–76]. For the kernel $\overline{\mathcal{K}}$ of Eq. (6) this entails, that the momentum-independent component $Z_1 \Gamma_\mu^{(0)}$ must be recast in terms of full vertices and propagators. To that end we resort to the standard skeleton expansion [30, 77].

There are two main steps employed in this procedure. First, the standard unrenormalized SDE for Γ is written such that all vertices in its diagrammatic representation are fully dressed. This is accomplished by modifying the corresponding multi-particle kernels appearing in the SDE, discarding graphs that would cause over-counting, such as ladder diagrams. Schematically, before renormalization, and displaying *only* graphs with quark-gluon vertices, we are led to

$$\Gamma = \Gamma^{(0)} + \int_k S \Gamma^{(0)} S M = \Gamma^{(0)} + \int_k S \Gamma S \tilde{M}, \quad (8)$$

where M is the SDE kernel, while \tilde{M} is the sum of all fully-dressed skeleton graphs, the first term being $\tilde{M}_1 = g^2 \Gamma \Delta \Gamma$. By virtue of this rearrangement, after renormalization, Z_1 appears

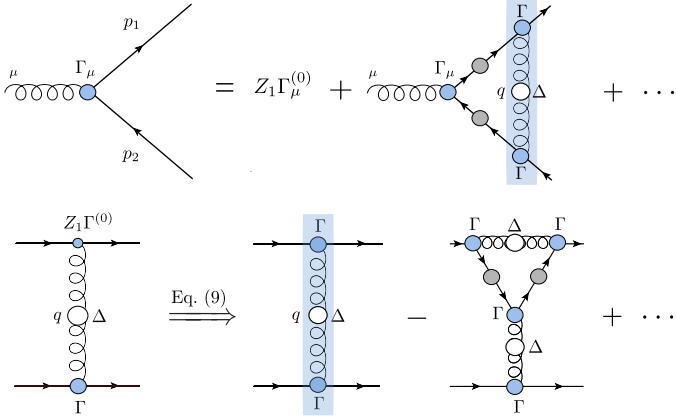


Figure 1: First row: the SDE of the quark-gluon vertex in the skeleton expansion; graphs with three- and four-gluon vertices are omitted. Second row: the one-gluon exchange kernel $\overline{\mathcal{K}}$ after the use of Eq. (9). The ellipses stand for higher order loop terms. White and grey circles denote fully-dressed gluon and quark propagators, respectively, while big (small) blue circles stand for fully-dressed (tree-level) quark-gluon vertices.

only multiplying the tree-level term $\Gamma^{(0)}$; thus, we get a dressed skeleton relation for $Z_1\Gamma^{(0)}$,

$$Z_1\Gamma^{(0)} = \Gamma - g^2 \int_k S \Gamma S \Gamma \Delta \Gamma + \dots, \quad (9)$$

where the ellipsis indicates (a) one-loop dressed graphs with three-gluon and four-gluon vertices, and (b) higher order diagrams in the skeleton expansion; they are all comprised exclusively by fully-dressed renormalized propagators and vertices.

The second step of the procedure is to use Eq. (9) into Eq. (6); this generates a form for $\overline{\mathcal{K}}$ which is expressed solely in terms of fully-dressed propagators and vertices, to wit

$$\overline{\mathcal{K}} = g^2 \Gamma_\mu(-q, p) \Delta^{\mu\nu}(q) \Gamma_\nu(q, k) - \dots, \quad (10)$$

as shown in Fig. 1. When the substitution captured by Fig. 1 is implemented on the system of the gap equation, the meson BSE, and the SDE of the axial-vector vertex, one obtains the system shown in Fig. 2, where $\overline{\mathcal{K}}$ (depicted as a blue box) is a common ingredient.

The ellipses indicate higher terms in the dressed-loop expansion, which will be neglected within the present truncation scheme. In fact, such additional terms may be interpreted as a systematic RG-improvement; this highlights that the above expansion naturally implements scaling properties, and, in particular, accommodates infrared momentum scaling relevant in the presence of soft (light) modes. We note in passing that the aforementioned rearrangements may also be derived within the framework of n -particle irreducible effective actions, see *e.g.*, [44, 78–84], or from the functional renormalization group approach [85].

4. Interaction strengths

The accuracy and reliability of the results obtained in the expansion scheme described in Sec. 3 hinges on the quantitative determination of the one-gluon exchange scattering kernel

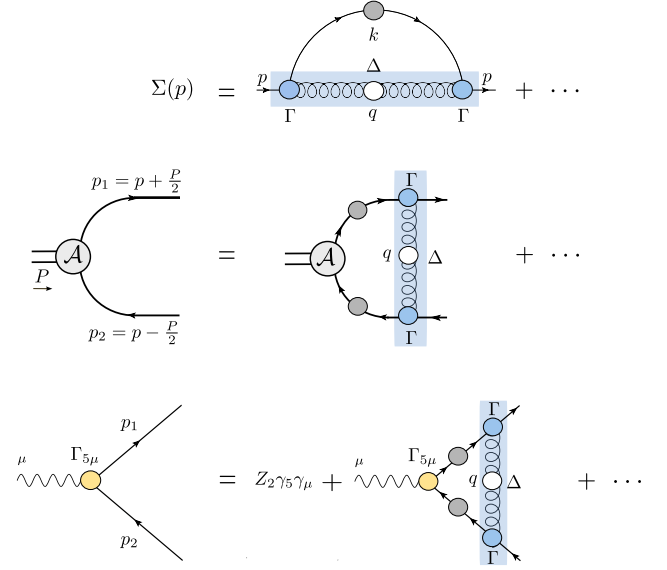


Figure 2: The quark gap equation (first row), the meson BSE (second row), and the SDE of the axial-vector vertex (third row), after the implementation of Eq. (9). The yellow circle indicates the axial-vector vertex, the wavy line represents a conserved axial-vector current, and the ellipses denote higher order terms in the skeleton expansion.

Eq. (10) that governs all equations, see the blue elongated boxes in Fig. 2. The two quark-gluon vertices appearing in Eq. (10) have a double effect on the relevant dynamics: (i) their flavour-independent part, identified through a judicious use of the corresponding STI, modifies the universal part of the interaction, amplifying the strength of the standard Taylor effective charge, $\alpha_\tau(q^2)$, and (ii) their flavour-dependent parts make the resulting interaction sensitive to the type of quarks involved in a given amplitude.

This analysis, while crucial for the quantitative precision and reliability of the current approach, is rather technical; we therefore highlight the important results: First, the STI allows us to determine the full universal part of the interaction strength as a combination of the Taylor coupling and the universal scalar dressing of the quark-ghost scattering kernel, see Eq. (19). Second, the flavour-dependent part is simply provided by powers of the quark wave functions $A_f(q)$, see Eq. (21). In combination this leads us to the one-gluon scattering kernel of Eq. (23).

We proceed with the derivation of these relations. Evidently, a central ingredient in this analysis is the STI for the quark-gluon vertex [59, 60],

$$q_\mu \Gamma_f^\mu(q, p) = F(q^2) \left[S_f^{-1}(r) H_f(q, p) - \overline{H}_f(-q, r) S_f^{-1}(p) \right], \quad (11)$$

where H_f denotes the composite operator known as the ghost-quark scattering kernel (see Fig. 3), corresponding to the quark of flavour f ; \overline{H} is the “conjugate” quantity, obtained from H_f following a set of standard rules, see *e.g.*, [86, 87]. The Lorentz decomposition of H_f is given by [86]

$$H_f(q, p) = X_0^f 1 + X_1^f \not{p} + X_2^f \not{p} + X_3^f \sigma_{\mu\nu} r^\mu p^\nu, \quad (12)$$

with the form factors $X_n^f := X_n^f(q^2, p^2, r^2)$, $n = 0, 1, 2, 3$.

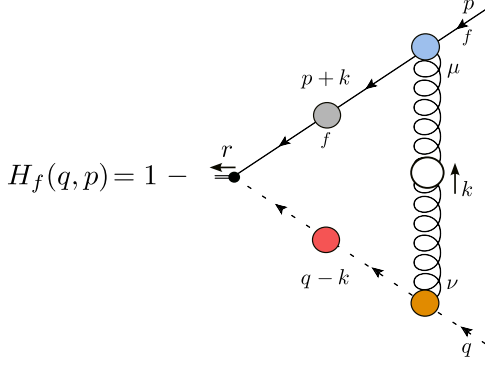


Figure 3: The quark-ghost scattering kernel at the one-loop dressed level. The red and orange circles denote the fully-dressed ghost propagator and ghost-gluon vertex, respectively.

We will next keep only the classical form factor of the quark-gluon vertex, namely

$$\Gamma_f^\mu(q, p) = \lambda_f(q, p)\gamma^\mu + \dots, \quad (13)$$

with the ellipsis denoting the remaining seven tensorial components. As is well-known, $\lambda_f(q, p)$ may be expressed in terms of the components appearing on the r.h.s of Eq. (11); in particular, setting $s^2 := r^2 + r \cdot p$ (see Eq. (3.5) in [88])

$$\lambda_f = \frac{1}{2}F(q^2) \left[A_f(r^2)(X_0^f - s^2 X_3^f) + B_i(r^2)(X_2^f - X_1^f) \right] + \dots \quad (14)$$

where the ellipsis denotes the “conjugate” expression, with $r \rightarrow p$. Given that the $X_{1,2,3}^f$ are numerically subleading [89], an excellent approximation to $\lambda_f(q, p)$ is achieved by retaining in Eq. (14) only the form factor X_0^f .

At this point, one notices already the emergence of the Taylor effective charge, $\alpha_r(q^2)$, defined in Eq. (4), being formed as a combination of the gluon propagator and the two factors $F(q^2)$ coming from each vertex. This term is usually referred to as “universal” or “process-independent”, since its form does not depend on the details of the specific process studied.

We next evaluate $\lambda_f(q, p)$ in the *symmetric* configuration, namely $q^2 = p^2 = r^2$. Denoting the resulting function by $\lambda_f^{\text{sym}}(q^2)$, Eq. (14) turns into

$$\lambda_f^{\text{sym}}(q^2) = F(q^2)A_f(q^2)X_0^f(q^2), \quad (15)$$

where half of the right hand side comes from the conjugate expression. The determination of $X_0^f(q^2)$ through the equation represented by the diagram of Fig. 3 requires knowledge of the quark propagator; the full treatment would therefore entail the coupling of this diagram to the quark gap equation. However, it turns out that $X_0^f(q^2)$ contains a flavour-independent part, to be denoted by $\tilde{X}_0(q^2)$, which emerges when the longitudinal part $k_\mu k_\nu$ of the gluon propagator $\Delta_{\mu\nu}(k)$ in Fig. 3 gets contracted with the quark-gluon vertex [blue circle], triggering the STI of Eq. (11). In particular, after setting $H = 1$, Eq. (11) furnishes a term $F(k)S_f^{-1}(k+p)$, which removes the internal quark propagator $S_f(k+p)$, yielding the f -independent contribution $\tilde{X}_0(q^2)$.

With these observations it follows straightforwardly that

$$\tilde{X}_0(q^2) = 1 - \frac{1}{2}g^2 N_c \int_k (k \cdot q) \Delta(k^2) D(k^2) B_1(k^2) D(t^2), \quad (16)$$

where $t = k+q$ and N_c the number of colours ($N_c = 3$). $B_1(k^2)$ is the tree-level form factor of the ghost-gluon vertex Γ_{cg} [orange circle in Fig. 3], renormalized in the Taylor scheme [59, 62, 90] ($Z_{cg} = 1$), and evaluated in the symmetric configuration.

We emphasize that the right hand-side of Eq. (16) is RGI and hence does not change under renormalization. Specifically, employing the relations $\Delta_r(q^2) = Z_A^{-1} \Delta(q^2)$, $D_r(q^2) = Z_c^{-1} D(q^2)$, $g_r = Z_A^{1/2} Z_c g$, and $Z_{cg} = 1$, we find

$$g^2 \Delta(k^2) D(k^2) B_1(k^2) D(t^2) = g_r^2 \Delta_r(k^2) D_r(k^2) B_1^r(k^2) D_r(t^2). \quad (17)$$

The upshot of the above considerations is to motivate the substitution $X_0^f(q^2) \rightarrow \tilde{X}_0(q^2)$ inside Eq. (15). This leads us to

$$\lambda_f^{\text{sym}}(q^2) = F(q^2) \tilde{X}_0(q^2) A_f(q^2), \quad (18)$$

where the entire flavour-dependence is contained in $A_f(q^2)$.

The kernel $\bar{\mathcal{K}}_{ff'}$ in Eq. (10) is constructed from the vertex contributions and the gluon propagator. Then, its process-independent part corresponds to a modification of the Taylor effective charge given in Eq. (4). Specifically, the inclusion of a factor $\tilde{X}_0(q^2)$ from each quark-gluon vertex leads to the new effective charge,

$$\tilde{\alpha}_r(q^2) = \alpha_r(q^2) \tilde{X}_0(q^2). \quad (19)$$

Note that, since both $\alpha_r(q^2)$ and $\tilde{X}_0(q^2)$ are RGI, so is the modified Taylor coupling $\tilde{\alpha}_r(q^2)$.

The determination of $\tilde{\alpha}_r(q^2)$ proceeds by providing the components $\alpha_r(q^2)$ and $\tilde{X}_0(q^2)$ of Eq. (19). For $\alpha_r(q^2)$ we use the lattice data of [65], obtained by combining $N = 2 + 1 + 1$ gluon and ghost propagators according to Eq. (4), see Fig. 4. The ghost-quark component $\tilde{X}_0(q^2)$ is obtained from Eq. (16), where the lattice results of [65] for $\Delta(k^2)$ and $D(k^2)$ are employed. $B_1(k^2)$ is computed from Eq.(4.5) of [67], after the appropriate inclusion of quark effects. Finally, the coupling α_s used in Eq. (16) is the central value of $\alpha_T(q)$ at $q = 4.3$ GeV, extracted from the orange curve in Fig. 4 (denoted by a “star”), namely $\alpha_T(4.3\text{GeV}) = 0.354 \pm 0.007$. We stress that the above determination of $\tilde{\alpha}_r(q^2)$ contains *no* adjustable parameters.

For computational convenience, the resulting curve of $\tilde{\alpha}_r(q^2)$, shown in Fig. 4 (red line), is fitted using the functional form,

$$\tilde{\alpha}_r(q^2) = \frac{a_0 q^2 + a_1 q^4 \ln\left(1 + \frac{\Lambda_0^2}{q^2}\right) + a_2 q^4}{1 + a_3 q^2 + a_4 q^4 + a_5 q^6} + \frac{4\pi q^6}{\beta_0 \left(\Lambda_0^6 + q^6 \ln \frac{q^2}{\Lambda_T^2}\right)}, \quad (20)$$

with the values $a_0 = 10.35$ GeV⁻², $a_1 = 23.69$ GeV⁻⁴, $a_2 = 27.94$ GeV⁻⁴, $a_3 = 10.72$ GeV⁻², $a_4 = -2.5$ GeV⁻⁴ and $a_5 = 29.02$ GeV⁻⁶. Additionally, $\Lambda_T = 0.5$ GeV, $\Lambda_0 = 1$ GeV and $\beta_0 = 11 - 2n_f/3$ ($n_f = 4$).

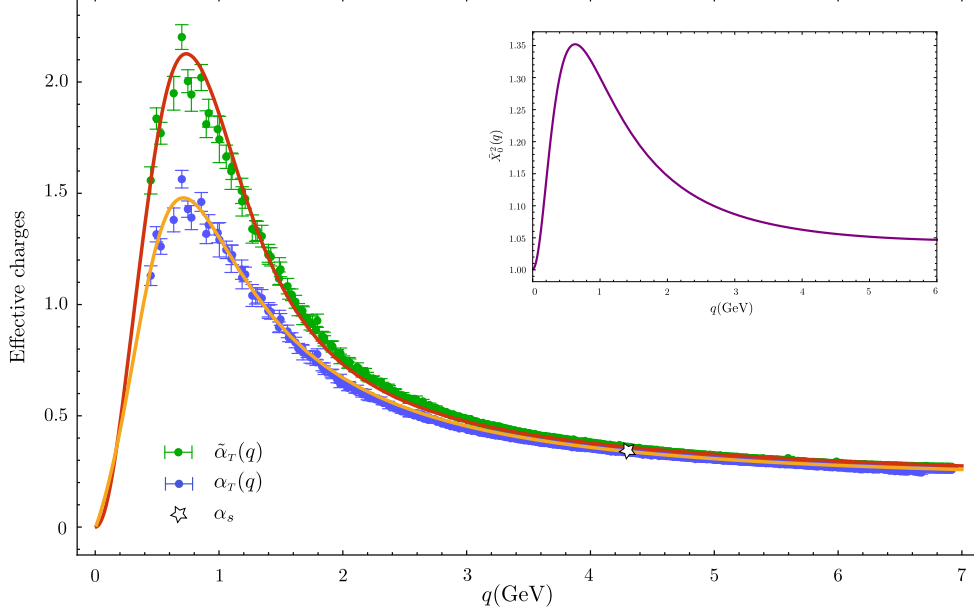


Figure 4: The lattice data of [65] for the Taylor effective charge, $\alpha_T(q^2)$ (blue data points, with orange continuous line as their fit), and the modified Taylor effective charge, $\tilde{\alpha}_T(q^2)$, [green data points], obtained from the $\alpha_T(q^2)$ data through multiplication by $\tilde{X}_0^2(q^2)$, according to Eq. (19). The red continuous line represents the fit of $\tilde{\alpha}_T(q^2)$ given by Eq. (20). The inset shows the function $\tilde{X}_0^2(q^2)$, computed by evaluating Eq. (16). Finally, the “star” marks the value $\alpha_T(4.3\text{GeV})$.

Once $\tilde{\alpha}_T(q^2)$ has been determined, the incorporation of $A_f(q^2)$ and $A_{f'}(q^2)$ from each vertex gives rise to the full *flavour-dependent* interaction,

$$\mathcal{I}_{ff'}(q^2) = \tilde{\alpha}_T(q^2)A_f(q^2)A_{f'}(q^2). \quad (21)$$

We emphasize that, in contradistinction to $\alpha_T(q^2)$ and $\tilde{\alpha}_T(q^2)$, the $\mathcal{I}_{ff'}(q^2)$ is *not* RG-invariant; specifically, we have that

$$\mathcal{I}_{ff'}^R(q^2) = Z_{2,f}^{-1}Z_{2,f'}^{-1}\mathcal{I}_{ff'}(q^2). \quad (22)$$

Then, the kernel $\overline{\mathcal{K}}_{ff'}$, given in Eq. (10), may be expressed in terms of the interaction $\mathcal{I}_{ff'}(q^2)$ according to

$$\overline{\mathcal{K}}_{ff'} = 4\pi\gamma^\mu\mathcal{I}_{ff'}(q^2)\gamma^\nu\Delta_{\mu\nu}^{(0)}(q). \quad (23)$$

We may now cast both Eq. (5) and Eq. (7) in terms of $\mathcal{I}_{ff'}(q^2)$, namely

$$S_f^{-1}(p) = Z_{2,f}(i\not{p} + m_f) + 4\pi C_F \int_k \gamma^\mu S_f(k)\gamma^\nu\Delta_{\mu\nu}^{(0)}(q)\mathcal{I}_{ff'}(q^2) \quad (24)$$

and

$$\mathcal{A}_{ff'}(p, P) = -4\pi \int_k \gamma^\mu \tilde{\mathcal{A}}_{ff'}(k, P)\gamma^\nu\Delta_{\mu\nu}^{(0)}(q)\mathcal{I}_{ff'}(q^2), \quad (25)$$

while, for the BSE of the vector mesons, we simply set $\mathcal{A}(p, P) \rightarrow \mathcal{A}_\mu(p, P)$ at the level of Eq. (25). We note that, since $\tilde{\mathcal{A}}(k, P) = S(k_1)\mathcal{A}(k, P)S(k_2)$, the full kernel of Eq. (25) is RGI by virtue of Eq. (22), as it should.

We end this section by stressing that the procedure leading to Eq. (24) and Eq. (25) is *symmetry preserving*, in the sense that the WTI satisfied by the axial-vector vertex, $\Gamma_{5\mu}^f(p_1, p_2)$, in the chiral limit [91], *i.e.*,

$$P^\mu\Gamma_{5\mu}^f(p_1, p_2) = S_f^{-1}(p_1)\gamma_5 + \gamma_5 S_f^{-1}(p_2), \quad (26)$$

is exactly fulfilled, with f a flavour index. Indeed, in the one-loop dressed approximation, the SDE of this vertex involves precisely the kernel $\mathcal{I}_{ff'}(q^2)$, namely

$$\Gamma_{5\mu}^f(p_1, p_2) = \gamma_5\gamma_\mu - 4\pi \int_k \gamma^\alpha \tilde{\Gamma}_{5\mu}^f(k_1, k_2)\gamma^\beta\Delta_{\alpha\beta}^{(0)}(q)\mathcal{I}_{ff'}(q^2), \quad (27)$$

with $\tilde{\Gamma}_{5\mu}^f(k_1, k_2) = S_f(k_1)\Gamma_{5\mu}^f(k_1, k_2)S_f(k_2)$. Consequently, the contraction of both sides of Eq. (27) by P^μ , and the use of Eq. (26) under the integral sign, returns precisely the difference of two quark self-energies [*viz.* Eq. (24)], exactly as happens in the case of the rainbow-ladder approximation. Clearly, this demonstration goes through because (i) the kernel $\mathcal{I}_{ff'}(q^2)$ is *common* to both Eq. (24) and Eq. (27), and (ii) due to the choice of the *symmetric limit*, its momentum dependence is the same as that of the gluon propagator. The preservation of Eq. (26) guarantees the vanishing of the pion mass in the chiral limit [30, 66], which is confirmed explicitly in the numerical analysis below.

We emphasize, however, that, in the presence of non-vanishing current quark masses, m_f and $m_{f'}$, the generalized WTI identity (see Eq.(2.5) in [92]) is not satisfied by the interaction $\mathcal{I}_{ff'}(q^2)$ in Eq. (21); for a symmetry-preserving treatment with a vertex solely depending on the gluon momentum see e.g. [93]. The violations are proportional to $|m_f - m_{f'}|$, which can be easily established by repeating the steps listed below Eq. (27), and noting that the term $A_f(q^2)A_{f'}(q^2)$ may not be assigned to the self-energy of either $S_f(p_1)$ or $S_{f'}(p_2)$. A consequence of the above structure are deviations from the Gell-Mann–Oakes–Renner relation [94], which is part of the systematic error of the current approximation.

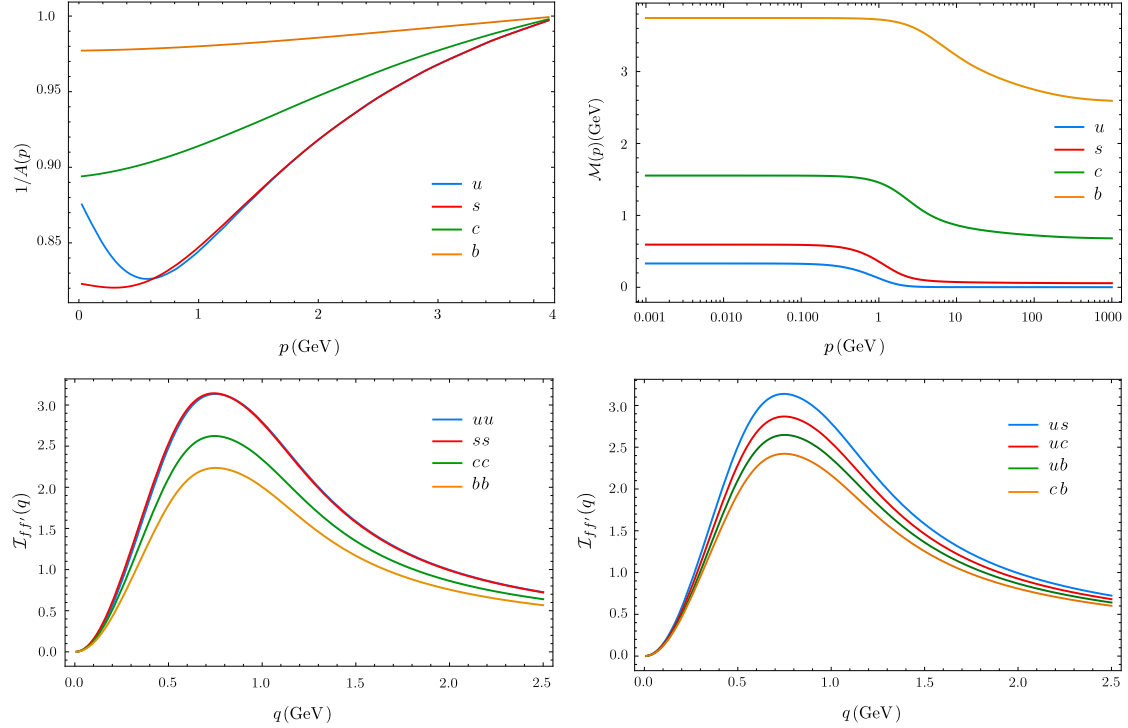


Figure 5: The inverses of the quark wave functions (upper left); the constituent quark masses $\mathcal{M}(p^2)$ (upper right); direct comparison of the four interaction strengths $\mathcal{I}_{ff}(q^2)$ (lower left); comparison between $\mathcal{I}_{uu}(q^2)$, $\mathcal{I}_{cc}(q^2)$, and $\mathcal{I}_{cu}(q^2)$ (lower right).

5. Results

In this section we use the two main dynamical equations, Eq. (24) and Eq. (25), to evaluate the ground-state masses of both light and heavy-light mesons, along with the corresponding decay constants, given by [66, 95],

$$\begin{aligned}
 f_{\text{ps}} m_{\text{ps}}^2 &= \sqrt{N_c} Z_2 \text{Tr} \int_k \gamma^5 \not{P} S(k_1) \mathcal{A}(k, P) S(k_2), \\
 f_{\text{v}} m_{\text{v}} &= \frac{\sqrt{N_c}}{3} Z_2 \text{Tr} \int_k \gamma_\mu S(k_1) \mathcal{A}_\mu(k, P) S(k_2), \quad (28)
 \end{aligned}$$

Before entering into the technicalities of the numerical treatment, we briefly comment on the renormalization procedure. After taking the appropriate traces, Eq. (24) yields two coupled integral equations for $A_f(p^2)$ and $B_f(p^2)$. These quantities depend on the renormalization constants Z_2 and Z_m , to be fixed by employing a specific renormalization scheme. In particular, in the standard momentum subtraction (MOM) scheme with the renormalization point $p^2 = \mu^2$, one imposes the conditions

$$A_f(\mu^2) = 1, \quad B_f(\mu^2) = m_f, \quad (29)$$

which, in turn, provide expressions for Z_2 and Z_m in terms of integrals evaluated at $q^2 = \mu^2$. The value of the μ chosen for the actual calculations is $\mu = 4.3$ GeV. Note that, while $\mathcal{M}_i(p^2)$ is RGI, the μ -dependence of $A_f(q^2)$ is transmitted to the interaction strength $\mathcal{I}_{ff}(q^2)$, which also depends on μ .

The central quantity appearing in both Eq. (24) and Eq. (25) is the flavour-dependent interaction $\mathcal{I}_{ff}(q^2)$ of Eq. (21). Importantly, the components that carry the dependence on the

flavour, namely $A_f(q^2)$ and $A_{f'}(q^2)$, are dynamically determined by solving Eq. (25).

The numerical procedure adopted is summarized below; for a detailed description of the numerical techniques and algorithms, the reader is referred to [96, 97]:

(a) In Euclidean space-time, the total momentum P of a bound state of mass M is parametrized as $P = (0, 0, 0, iM)$, where $P^2 = -M^2$. Then, the arguments of the quark propagators $S(k_{1,2})$ appearing in the BS equation satisfy $k_{1,2}^2 = k^2 + P^2/4 \pm k \cdot P$, corresponding to parabolas in the complex plane formed by k_1 and k_2 . The analytic continuation of the gap equation to the complex plane is achieved using the Cauchy interpolation method [97–99]. The range of its applicability is restricted by the appearance of complex conjugate poles in $S(k_{1,2})$; their exact position, and the maximum mass that can be extracted, depend on the values of the current quark masses, m_i .

(b) The procedure adopted for fixing the current quark masses, as well as the pion and η -meson masses, is as follows. First, we compute the quark propagator for a given current quark mass on the complex plane, using the Cauchy interpolation method. Since the pion mass lies within the computable region of the propagator, the u and d masses, assumed to be equal, can be easily adjusted to reproduce the experimental value. In the case of the η meson, its mass lies in a region where the quark propagator cannot be directly computed, due to the presence of complex poles. Therefore, for that region, an Ansatz containing a pair of complex conjugate poles is used,

mass (GeV)	π	K	ρ	D	D^*	D_s	D_s^*	B	B^*	B_s	B_s^*	B_c	B_c^*	η_c	J/Ψ	η_b
This work	0.139 [†]	0.495 [†]	0.735	1.93	2.06	2.03	2.17	5.33	5.37	5.45	5.48	6.36	6.40	2.97 [†]	3.13	9.5 [†]
Experiment [100]	0.139	0.494	0.775	1.87	2.01	1.97	2.11	5.28	5.33	5.37	5.42	6.28		2.98	3.10	9.4
% deviation			5.1	3.2	2.5	3.0	2.8	0.9	0.7	1.5	1.1	1.3			1.0	
Lattice [101–105]				1.86	2.01	1.97	2.11	5.28	5.32	5.37	5.42	6.26	6.33		3.12	

Table 1: Meson masses, all results are presented in GeV. The free parameters have been fixed to reproduce the values denoted with a †.

f (GeV)	π	K	ρ	D	D^*	D_s	D_s^*	B	B^*	B_s	B_s^*	B_c	B_c^*	η_c	J/Ψ	η_b
This work	0.130 [†]	0.158	0.205	0.201	0.218	0.249	0.270	0.201	0.197	0.235	0.231	0.505	0.492	0.355	0.433	0.762
Experiment [100]	0.130	0.155	0.212	0.196		0.236		0.211						0.340	0.415	
% deviation		1.9	3.3	2.6		5.5		4.7						4.4	4.0	
ETM [101]				0.208	0.223	0.247	0.268	0.193	0.186	0.229	0.223					
MILC18 [106]				0.213		0.245		0.189		0.231						
HPQCD [105, 107–109]	0.132	0.157		0.207		0.241		0.189		0.231		0.427	0.422	0.395	0.404	
RBC/UKQCD [110, 111]				0.209		0.246		0.196		0.235						

Table 2: Decay constants, all results are presented in GeV. The free parameters have been fixed to reproduce the values denoted with a †. In our normalization, $f_\pi = 0.130$ GeV.

namely [112, 113],

$$\begin{aligned}
S(p) &= -i\not{p}\sigma_v(p^2) + \sigma_s(p^2), \\
\sigma_v(p^2) &= \sum_i^n \left[\frac{\alpha_i}{p^2 + m_i} + \frac{\alpha_i^*}{p^2 + m_i^*} \right], \\
\sigma_s(p^2) &= \sum_i^n \left[\frac{\beta_i}{p^2 + m_i} + \frac{\beta_i^*}{p^2 + m_i^*} \right], \quad (30)
\end{aligned}$$

where the parameters m_i , α_i , and β_i are derived by fitting the respective quark SDE solution along the parabolic trajectory in the complex plane. If the calculated bound state mass for the chosen current quark mass fails to reproduce the η meson mass, the entire procedure must be iterated, for a new set of quark masses. The current quark masses obtained through this procedure are $m_{u/d} = 0.005$ GeV, $m_s = 0.094$ GeV, $m_c = 1.1$ GeV, and $m_b = 3.5$ GeV, at $\mu = 4.3$ GeV.

(c) The BS equation is solved numerically by reformulating it into an eigenvalue problem. Physical solutions correspond to the mass-shell points $P_n^2 = -M_n^2$, where M_0^2 denotes the ground state mass of the meson, and M_n^2 ($n \geq 1$) represents the n^{th} radial excitation. Furthermore, the calculation of meson BS amplitudes is simplified by expanding them into Chebyshev polynomials of the second kind, thus facilitating the factorization of the angular dependence. For the calculation of all meson BS amplitudes (both pseudoscalar and vector particles), we have employed a total of 10 such polynomials. We remark that, in the case of the heavy-light mesons, the significant differences in quark masses require high precision to ensure convergence. In particular, we have employed a total of 160

integration points for the relative momentum k and 48 points for the angular variables. Additionally, the heavy-light and heavy-heavy meson masses have been computed employing the quark parametrization from Eq. (30).

The results of this analysis may be summarized as follows:

(i) The inverse quark wave functions $A_f^{-1}(p^2)$ for $f = u, s, c, b$ are shown in the left upper panel of Fig. 5; the case $f = d$ coincides with that of u , and is omitted. We note that $A_u^{-1}(p^2)$ displays the typical minimum, which is hardly visible in $A_s^{-1}(p^2)$, and absent in $A_c^{-1}(p^2)$ and $A_b^{-1}(p^2)$; again, $\mu = 4.3$ GeV.

(ii) The dynamically generated quark masses $\mathcal{M}_i(p^2)$ are shown in the upper right panel of Fig. 5. The corresponding values at the origin are $\mathcal{M}_u(0) = 0.34$ GeV, $\mathcal{M}_s(0) = 0.59$ GeV, $\mathcal{M}_c(0) = 1.55$ GeV, and $\mathcal{M}_b(0) = 3.78$ GeV.

(iii) The diagonal elements, $f = f'$, of the flavour-dependent interaction strength $\mathcal{I}_{ff'}(q^2)$, are shown in the lower left panel of Fig. 5, for $f = u, s, c, b$, and with $\mu = 4.3$ GeV. Note that $\mathcal{I}_{uu}(q^2) \approx \mathcal{I}_{ss}(q^2)$. As expected, the intensity of the interaction decreases when heavier quarks are considered, *i.e.*, $\mathcal{I}_{bb}(q^2) < \mathcal{I}_{cc}(q^2) < \mathcal{I}_{ss}(q^2)$ for all momenta except the origin, where $\mathcal{I}_{ff'}(0) = 0$ for all cases. Furthermore, in the lower right panel of Fig. 5 we show some of the non-diagonal elements. Comparison with the curves in the lower left panel reveals that, as expected, $\mathcal{I}_{cc}(q^2) < \mathcal{I}_{cu}(q^2) < \mathcal{I}_{uu}(q^2)$, with analogous relations for all other combinations considered.

(iv) The masses and decay constants of 16 states are shown in Tables 1 and 2, respectively, where they are compared with the corresponding experimental and lattice values, whenever

available. We find excellent agreement, reflected in the small percentage deviations reported, which do not exceed the few percent level. The most notable exceptions are the decay constants of B_c , B_c^* and η_c , whose relative deviations from the lattice results are 18%, 17%, and 10%, respectively.

(v) Finally, we have computed the masses of the first radial excitations for the pion and kaon, obtaining $m_{\pi_1} = 1.24\text{GeV}$ and $m_{K_1} = 1.30\text{GeV}$, compared with the experimental values of $m_{\pi_1}^{\text{exp}} = 1.30\text{GeV}$ and $m_{K_1}^{\text{exp}} = 1.46\text{GeV}$ [100]. Note that the above mass hierarchy is typically inverted within the rainbow-ladder approximation, requiring the inclusion of the anomalous chromomagnetic moment for its restoration [93, 114].

6. Conclusions

In this work we have introduced a novel expansion scheme for functional bound state equations on the basis of a four-quark kernel solely derived from QCD correlation functions: The two main building blocks of this kernel are a universal flavour-independent effective charge, see Eq. (19), and flavour-dependent contributions in terms of the quark dressings, leading to the final kernel Eq. (21). These two central quantities can either be obtained self-consistently from solutions of functional approaches to QCD, or from lattice simulations.

The quantitative precision of this scheme has been established within the computation of masses and decay constants of heavy-light mesons, see Tables 1 and 2. We envisage its application to a broad range of applications, and in particular on electromagnetic meson form factors and parton distribution amplitudes. Moreover, while improving the expansion scheme beyond the present single gluon exchange approximation in a symmetry-preserving way proves challenging, we hope to report on this in the near future.

Acknowledgements

We thank G. Eichmann, M.N. Ferreira and J. Rodriguez-Quintero for discussions. The work of A.S.M. and J.P. is funded by the Spanish MICINN grants PID2020-113334GB-I00 and PID2023-151418NB-I00, the Generalitat Valenciana grant CIPROM/2022/66, and CEX2023-001292-S by MCIU/AEI. J.P. is supported in part by the EMMI visiting grant of the ExtreMe Matter Institute EMMI at the GSI, Darmstadt, Germany. F.G. is supported by the National Science Foundation of China under Grants No. 12305134. J.M.P. is funded by the Deutsche Forschungsgemeinschaft (DFG, German Research Foundation) under Germany's Excellence Strategy EXC 2181/1 - 390900948 (the Heidelberg STRUCTURES Excellence Cluster) and the Collaborative Research Centre SFB 1225 - 273811115 (ISOQUANT).

References

[1] M. A. Ivanov, Y. L. Kalinovsky, C. D. Roberts, Phys. Rev. D 60 (1999) 034018.
[2] M. S. Bhagwat, A. Krassnigg, P. Maris, C. D. Roberts, Eur. Phys. J. A 31 (2007) 630–637.

[3] M. Gomez-Rocha, T. Hilger, A. Krassnigg, Phys. Rev. D 92 (5) (2015) 054030.
[4] C. S. Fischer, S. Kubrak, R. Williams, Eur. Phys. J. A 51 (2015) 10.
[5] M. Chen, L. Chang, Chin. Phys. C 43 (11) (2019) 114103.
[6] P. Qin, S.-x. Qin, Y.-x. Liu, Phys. Rev. D 101 (11) (2020) 114014.
[7] T. Hilger, C. Popovici, M. Gomez-Rocha, A. Krassnigg, Phys. Rev. D 91 (3) (2015) 034013.
[8] T. Nguyen, N. A. Souchlas, P. C. Tandy, AIP Conference Proceedings 1116 (1) (2009) 327–333.
[9] N. Souchlas, Phys. Rev. D 81 (2010) 114019.
[10] D. Binosi, L. Chang, M. Ding, F. Gao, J. Papavassiliou, C. D. Roberts, Phys. Lett. B 790 (2019) 257–262.
[11] P. Gelhausen, A. Khodjamirian, A. A. Pivovarov, D. Rosenthal, Phys. Rev. D 88 (2013) 014015, [Erratum: Phys.Rev.D 89, 099901 (2014), Erratum: Phys.Rev.D 91, 099901 (2015)].
[12] J.-B. Liu, M.-Z. Yang, Chin. Phys. C 40 (7) (2016) 073101.
[13] Z.-G. Wang, Eur. Phys. J. C 75 (2015) 427.
[14] S. Tang, Y. Li, P. Maris, J. P. Vary, Eur. Phys. J. C 80 (6) (2020) 522.
[15] H. Mutuk, Adv. High Energy Phys. 2018 (2018) 8095653.
[16] B. Aubert, et al., Phys. Rev. Lett. 90 (2003) 242001.
[17] D. Besson, et al., Phys. Rev. D 68 (2003) 032002, [Erratum: Phys.Rev.D 75, 119908 (2007)].
[18] P. Krokovny, et al., Phys. Rev. Lett. 91 (2003) 262002.
[19] B. Aubert, et al., Phys. Rev. D 69 (2004) 031101.
[20] M. Di Pierro, E. Eichten, Phys. Rev. D 64 (2001) 114004.
[21] G. Barucca, et al., Eur. Phys. J. A 57 (6) (2021) 184.
[22] R. Aaij, et al., JHEP 04 (2024) 151.
[23] L. Capriotti, J. Phys. Conf. Ser. 1137 (1) (2019) 012004.
[24] M. Ablikim, et al., Phys. Rev. Lett. 131 (15) (2023) 151903.
[25] A. M. Sirunyan, et al., Phys. Rev. Lett. 122 (13) (2019) 132001.
[26] P. Jain, H. J. Munczek, Phys. Rev. D 48 (1993) 5403–5411.
[27] R. Alkofer, P. Watson, H. Weigel, Phys. Rev. D 65 (2002) 094026.
[28] A. Bender, W. Detmold, C. Roberts, A. W. Thomas, Phys. Rev. C 65 (2002) 065203.
[29] L. Chang, C. D. Roberts, Phys. Rev. Lett. 103 (2009) 081601.
[30] C. D. Roberts, A. G. Williams, Prog. Part. Nucl. Phys. 33 (1994) 477–575.
[31] C. Savkli, F. Tabakin, Nucl. Phys. A 628 (1998) 645–668.
[32] P. Maris, C. D. Roberts, Int. J. Mod. Phys. E12 (2003) 297–365.
[33] P. Watson, W. Cassing, P. C. Tandy, Few Body Syst. 35 (2004) 129–153.
[34] G. Eichmann, R. Alkofer, I. C. Cloet, A. Krassnigg, C. D. Roberts, Phys. Rev. C 77 (2008) 042202.
[35] S.-x. Qin, L. Chang, Y.-x. Liu, C. D. Roberts, D. J. Wilson, Phys. Rev. C 84 (2011) 042202.
[36] C. S. Fischer, R. Williams, Phys. Rev. D 78 (2008) 074006.
[37] L. Chang, C. D. Roberts, Phys. Rev. C 85 (2012) 052201.
[38] H. L. L. Roberts, L. Chang, I. C. Cloet, C. D. Roberts, Few Body Syst. 51 (2011) 1–25.
[39] A. Bashir, L. Chang, I. C. Cloet, B. El-Bennich, Y.-X. Liu, et al., Commun. Theor. Phys. 58 (2012) 79–134.
[40] G. Eichmann, J. Phys. Conf. Ser. 426 (2013) 012014.
[41] W. Heupel, T. Goecke, C. S. Fischer, Eur. Phys. J. A50 (2014) 85.
[42] D. Binosi, L. Chang, J. Papavassiliou, C. D. Roberts, Phys. Lett. B742 (2015) 183–188.
[43] H. Sanchis-Alepuz, R. Williams, J. Phys. Conf. Ser. 631 (1) (2015) 012064.
[44] R. Williams, C. S. Fischer, W. Heupel, Phys. Rev. D93 (3) (2016) 034026.
[45] M. A. Bedolla, J. J. Cobos-Martínez, A. Bashir, Phys. Rev. D 92 (5) (2015) 054031.
[46] H. Sanchis-Alepuz, R. Williams, Phys. Lett. B749 (2015) 592–596.
[47] B.-L. Li, L. Chang, M. Ding, C. D. Roberts, H.-S. Zong, Phys. Rev. D 94 (9) (2016) 094014.
[48] D. Binosi, L. Chang, J. Papavassiliou, S.-X. Qin, C. D. Roberts, Phys. Rev. D93 (9) (2016) 096010.
[49] D. Binosi, C. D. Roberts, J. Rodriguez-Quintero, Phys. Rev. D 95 (11) (2017) 114009.
[50] F. E. Serna, B. El-Bennich, G. a. Krein, Phys. Rev. D 96 (1) (2017) 014013.
[51] A. S. Miramontes, H. Sanchis-Alepuz, Eur. Phys. J. A 55 (10) (2019) 170.

- [52] G. Eichmann, C. S. Fischer, W. Heupel, N. Santowsky, P. C. Wallbott, *Few Body Syst.* 61 (4) (2020) 38.
- [53] P. C. Wallbott, G. Eichmann, C. S. Fischer, *Phys. Rev. D* 102 (5) (2020) 051501.
- [54] A. S. Miramontes, H. Sanchis-Alepuz, R. Alkofer, *Phys. Rev. D* 103 (11) (2021) 116006.
- [55] L. X. Gutiérrez-Guerrero, G. Paredes-Torres, A. Bashir, *Phys. Rev. D* 104 (9) (2021) 094013.
- [56] P.-L. Yin, C. Chen, G. a. Krein, C. D. Roberts, J. Segovia, S.-S. Xu, *Phys. Rev. D* 100 (3) (2019) 034008.
- [57] G. Eichmann, A. Gómez, J. Horak, J. M. Pawłowski, J. Wessely, N. Wink, *Phys. Rev. D* 109 (9) (2024) 096024.
- [58] K. Raya, A. Bashir, D. Binosi, C. D. Roberts, J. Rodríguez-Quintero, *Few Body Syst.* 65 (2) (2024) 60.
- [59] W. J. Marciano, H. Pagels, *Phys. Rept.* 36 (1978) 137.
- [60] J. S. Ball, T.-W. Chiu, *Phys. Rev. D* 22 (1980) 2542.
- [61] L. von Smekal, R. Alkofer, A. Hauck, *Phys. Rev. Lett.* 79 (1997) 3591–3594.
- [62] P. Boucaud, F. De Soto, J. Leroy, A. Le Yaouanc, J. Micheli, et al., *Phys. Rev. D* 79 (2009) 014508.
- [63] L. von Smekal, K. Maltman, A. Sternbeck, *Phys. Lett. B* 681 (2009) 336–342.
- [64] B. Blossier, P. Boucaud, M. Brinet, F. De Soto, X. Du, V. Morenas, O. Pene, K. Petrov, J. Rodríguez-Quintero, *Phys. Rev. Lett.* 108 (2012) 262002.
- [65] S. Zafeiropoulos, P. Boucaud, F. De Soto, J. Rodríguez-Quintero, J. Segovia, *Phys. Rev. Lett.* 122 (16) (2019) 162002.
- [66] P. Maris, C. D. Roberts, P. C. Tandy, *Phys. Lett. B* 420 (1998) 267–273.
- [67] A. C. Aguilar, C. O. Ambrósio, F. De Soto, M. N. Ferreira, B. M. Oliveira, J. Papavassiliou, J. Rodríguez-Quintero, *Phys. Rev. D* 104 (5) (2021) 054028.
- [68] M. Mitter, J. M. Pawłowski, N. Strodthoff, *Phys. Rev. D* 91 (2015) 054035.
- [69] A. K. Cyrol, L. Fister, M. Mitter, J. M. Pawłowski, N. Strodthoff, *Phys. Rev. D* 94 (5) (2016) 054005.
- [70] A. K. Cyrol, M. Mitter, J. M. Pawłowski, N. Strodthoff, *Phys. Rev. D* 97 (5) (2018) 054006.
- [71] M. Q. Huber, *Phys. Rept.* 879 (2020) 1–92.
- [72] F. Gao, J. Papavassiliou, J. M. Pawłowski, *Phys. Rev. D* 103 (9) (2021) 094013.
- [73] M. N. Ferreira, J. Papavassiliou, *Particles* 6 (1) (2023) 312–363.
- [74] D. Binosi, J. Papavassiliou, *Phys. Rept.* 479 (2009) 1–152.
- [75] A. C. Aguilar, D. Binosi, J. Papavassiliou, J. Rodríguez-Quintero, *Phys. Rev. D* 80 (2009) 085018.
- [76] D. Binosi, C. Mezrag, J. Papavassiliou, C. D. Roberts, J. Rodríguez-Quintero, *Phys. Rev. D* 96 (5) (2017) 054026.
- [77] J. D. Bjorken, S. D. Drell, *Relativistic quantum fields*, International Series in Pure and Applied Physics, McGraw-Hill, New York, 1965.
- [78] G. Baym, L. P. Kadanoff, *Phys. Rev.* 124 (1961) 287–299.
- [79] J. Cornwall, R. Norton, *Phys. Rev. D* 8 (1973) 3338–3346.
- [80] J. M. Cornwall, R. Jackiw, E. Tomboulis, *Phys. Rev. D* 10 (1974) 2428–2445.
- [81] J. Berges, *Phys. Rev. D* 70 (2004) 105010.
- [82] R. Alkofer, C. S. Fischer, F. J. Llanes-Estrada, K. Schwenzer, *Annals Phys.* 324 (2009) 106–172.
- [83] M. E. Carrington, Y. Guo, *Phys. Rev. D* 83 (2011) 016006.
- [84] M. C. A. York, G. D. Moore, M. Tassler, *JHEP* 06 (2012) 077.
- [85] J. M. Pawłowski, *Annals Phys.* 322 (2007) 2831–2915.
- [86] A. I. Davydchev, P. Osland, L. Saks, *Phys. Rev. D* 63 (2001) 014022.
- [87] A. C. Aguilar, M. N. Ferreira, C. T. Figueiredo, J. Papavassiliou, *Phys. Rev. D* 99 (2019) 034026.
- [88] A. C. Aguilar, J. Papavassiliou, *Phys. Rev. D* 83 (2011) 014013.
- [89] A. C. Aguilar, J. C. Cardona, M. N. Ferreira, J. Papavassiliou, *Phys. Rev. D* 96 (1) (2017) 014029.
- [90] J. Taylor, *Nucl. Phys. B* 33 (1971) 436–444.
- [91] S.-X. Qin, C. D. Roberts, S. M. Schmidt, *Phys. Lett. B* 733 (2014) 202–208.
- [92] C. D. Roberts, *J. Phys. Conf. Ser.* 706 (2) (2016) 022003.
- [93] Z.-N. Xu, Z.-Q. Yao, S.-X. Qin, Z.-F. Cui, C. D. Roberts, *Eur. Phys. J. A* 59 (3) (2023) 39.
- [94] M. Gell-Mann, R. J. Oakes, B. Renner, *Phys. Rev.* 175 (1968) 2195–2199.
- [95] P. Maris, P. C. Tandy, *Phys. Rev. C* 60 (1999) 055214.
- [96] G. Eichmann, H. Sanchis-Alepuz, R. Williams, R. Alkofer, C. S. Fischer, *Prog. Part. Nucl. Phys.* 91 (2016) 1–100.
- [97] H. Sanchis-Alepuz, R. Williams, *Comput. Phys. Commun.* 232 (2018) 1–21.
- [98] C. Fischer, P. Watson, W. Cassing, *Phys. Rev. D* 72 (2005) 094025.
- [99] A. Krassnigg, *PoS CONFINEMENT8* (2008) 075.
- [100] R. L. Workman, et al., *PTEP* 2022 (2022) 083C01.
- [101] V. Lubicz, A. Melis, S. Simula, *Phys. Rev. D* 96 (3) (2017) 034524.
- [102] R. J. Dowdall, C. T. H. Davies, T. C. Hammant, R. R. Horgan, *Phys. Rev. D* 86 (2012) 094510.
- [103] K. Cichy, M. Kalinowski, M. Wagner, *Phys. Rev. D* 94 (9) (2016) 094503.
- [104] N. Mathur, M. Padmanath, S. Mondal, *Phys. Rev. Lett.* 121 (20) (2018) 202002.
- [105] G. C. Donald, C. T. H. Davies, R. J. Dowdall, E. Follana, K. Hornbostel, J. Koponen, G. P. Lepage, C. McNeile, *Phys. Rev. D* 86 (2012) 094501.
- [106] A. Bazavov, et al., *Phys. Rev. D* 98 (7) (2018) 074512.
- [107] C. T. H. Davies, C. McNeile, E. Follana, G. P. Lepage, H. Na, J. Shigemitsu, *Phys. Rev. D* 82 (2010) 114504.
- [108] C. Hughes, C. T. H. Davies, C. J. Monahan, *Phys. Rev. D* 97 (5) (2018) 054509.
- [109] C. McNeile, C. T. H. Davies, E. Follana, K. Hornbostel, G. P. Lepage, *Phys. Rev. D* 86 (2012) 074503.
- [110] P. A. Boyle, L. Del Debbio, A. Jüttner, A. Khamseh, F. Sanfilippo, J. T. Tsang, *J. High Energy Phys.* 12 (2017) 008.
- [111] N. H. Christ, J. M. Flynn, T. Izubuchi, T. Kawanai, C. Lehner, A. Soni, R. S. Van de Water, O. Witzel, *Phys. Rev. D* 91 (5) (2015) 054502.
- [112] E. Rojas, B. El-Bennich, J. P. B. C. de Melo, *Phys. Rev. D* 90 (2014) 074025.
- [113] F. F. Mojica, C. E. Vera, E. Rojas, B. El-Bennich, *Phys. Rev. D* 96 (1) (2017) 014012.
- [114] S.-X. Qin, C. D. Roberts, *Chin. Phys. Lett.* 38 (7) (2021) 071201.